Mechanical Properties of Flame Retardant Filled Polypropylene Composites

C. M. TAI, ROBERT K. Y. LI

Department of Physics and Materials Science, City University of Hong Kong, Tat Chee Avenue, Kowloon, Hong Kong

Received 3 June 2000; accepted 30 August 2000

ABSTRACT: The flammability performance and mechanical behaviors for halogen-based and non-halogen-based flame retardant (FR) filled polypropylene (PP) composites were investigated in this study. The halogen-based FR system consisted of a mixture of brominated phosphate ester and antimony trioxide (BR), and the halogen-free FR was a magnesium hydroxide (MH). It was found from limiting oxygen index measurements that 60 wt % of MH was needed in order to achieve the same degree of flammability as the composite containing only 30 wt % of BR. Scanning electron microscopy examinations of the fractured specimens indicated that the interfacial bond strength between PP and MH was stronger than that for PP and BR. The notched Charpy impact strength and the impact fracture toughness were measured and compared. The discrepancies between the two impact test results could be correlated after kinetic energy correction was applied to the Charpy impact strengths. © 2001 John Wiley & Sons, Inc. J Appl Polym Sci 80: 2718–2728, 2001

Key words: flammability; mechanical behavior; halogen; polypropylene

INTRODUCTION

Polymeric materials have become more widely used in areas such as home furnishings, construction, and various industrial applications. However, most polymers contain high carbon and hydrogen contents, which are flammable to various degrees. As a result, much attention has been paid to the flammability of polymers. The most commonly used method to control the flammability of polymers is the addition of flame retardant (FR) additives to the polymer matrix.[1]

The FRs are additives that are used to alter the burning rate of the base materials. Among the different types of FRs, halogenated organic compounds are well established for polymers. Halogens are effective because they interfere with the chemical chain reactions that propagate fire. The addition of antimony trioxides (Sb_2O_3) to halogen-based FRs would enhance the flame retardancy effectively. This is mainly due to the synergism between the halogenated compounds and antimony oxide to form volatile antimony halides that act as free radicals trapped around the flame.[2] However, such types of FRs are not thermally stable; they generate toxic gases and corrosive smokes during combustion or high temperature processing.[3] In relation to this, use of halogen-based FRs has given rise to some environmental concern.[4,5] Research for acid- and halogen-free FRs has become important.

Among the non-halogen-based FRs, magnesium hydroxides [$Mg(OH)_2$] have been studied in detail and represent the most popular replacements for halogen-based FRs. The mechanisms of $Mg(OH)_2$ as a FR are totally different from that of

Correspondence to: R. K. Y. Li (aprkyl@cityu.edu.hk).

Contract grant sponsor: Research Grants Council of the Hong Kong Special Administrative Region, China; contract grant number: 9040508.

Journal of Applied Polymer Science, Vol. 80, 2718–2728 (2001)

Table I Designation and Constituent Compositions for Materials

Sample Designation	Composition (wt %)		
	Polypropylene	Mixture of Brominated Phosphate Ester & Antimony Trioxide	Magnesium Hydroxide
PP	100	—	—
BR-10	90	10	—
BR-20	80	20	—
BR-30	70	30	—
MH-10	90	—	10
MH-20	80	—	20
MH-30	70	—	30
MH-40	60	—	40
MH-50	50	—	50
MH-60	40	—	60

a halogen-based FR. During combustion, $Mg(OH)_2$ undergoes endothermic decomposition, which withdraws heat from the substrates and hence retards the rate of thermal degradation. High loading of halogen-free FR is necessary to act as a solid-phase diluent for adequate flame retardancy.[6–9]

Among the studies on FR filled polymers, much attention has been paid to the development of FR materials. The mechanical properties of such material systems are considered less often. The objective of this study was to evaluate and compare the mechanical properties of polypropylene (PP) filled with halogenated and nonhalogenated FRs.

EXPERIMENTAL

Materials and Sample Preparation

A PP homopolymer (Pro-fax 6331, Montall) was used as the matrix material. Two types of FRs were employed in this study. One of the FR systems consisted of a mixture of brominated phosphate ester (grade Pb-370, FMC Corporation) and antimony trioxide (Sb_2O_3) in a weight ratio of 2:1; this mixture was designated as BR. The other FR was $Mg(OH)_2$ (Magnifin H5 grade, Martinswerk); this system was designated as MH. The maximum loading of FR employed was 30 wt % for the BR system and 60 wt % for the MH system. They were chosen because the respective maximum FR loading gives the required flammability performance. A summary of the compositions for the different PP/FR composites used in this study is given in Table I.

In the preparation of the FR filled PP composites, the respective virgin PP pellets and FR powders were dry mixed in the required ratio before compounding. The PP/FR mixtures were compounded by a twin-screw extruder attachment connected to a Brabender Plasticorder (PL2000). The extrudates were subsequently pelletized and injection molded into rectangular plates and dumbbell-shaped tensile bars under the same conditions.

Tensile Tests

Tensile tests were performed with an Instron tensile tester (model 4206) at a crosshead speed of 1 mm/min at room temperature. The geometry of the specimens was in accordance with the ASTM D638 type I standard. The samples had a gauge length, width, and thickness equal to 57, 12.7, and 3.2 mm, respectively. A clip-on extensometer with a gauge length of 12.5 mm was used to measure the tensile modulus. The results reported were the average from five samples.

Impact Fracture Tests

The impact fracture characteristics for the FR filled PP composites were measured by two methods: conventional Charpy impact tests and impact critical strain energy release rate (G_C) measurement via the linear elastic fracture mechanics (LEFM) approach. While the conventional pendulum impact tests are convenient and simple to

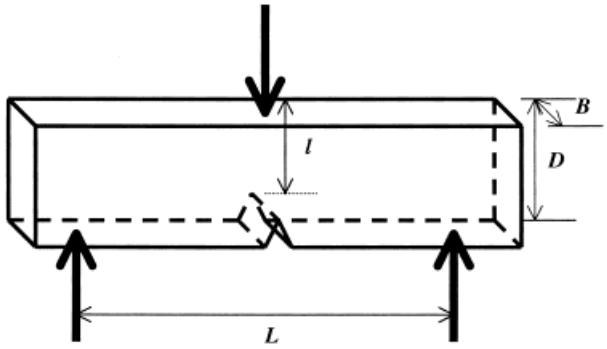

Figure 1 The single edge notched bend specimen geometry used in the impact tests.

carry out, the test results are specimen geometry dependent.[10] A more fundamental approach to characterize the fracture behavior of polymers is through the fracture mechanics approach.[11] The fracture toughness value obtained from the fracture mechanics analysis is a true material property that can be used as a yardstick for materials selection and a parameter for use in product design calculations.

Specimens having dimensions of 80 × 13 × 6 mm were cut from the molded rectangular plates for the Charpy impact test. Each specimen was provided with a 2 mm deep notch (≈ 0.25-mm notch tip radius) and tested by a Ceast Fractovis instrumented drop weight impact tester. The specimen geometry was similar to ASTM D256, except that the distance between the support span was 52 mm. The impact velocity was fixed at 4 m/s. The Charpy impact strength (S_I) is defined as the total energy (U) absorbed in the impact test divided by the ligament area (see Fig. 1).

$$S_I = \frac{U}{A_l} = \frac{U}{Bl} \quad (1)$$

where B and l are defined in Fig. 1.

Five tests were conducted and the average value was reported for each material system.

In the fracture mechanics characterization of materials, depending on the mode of failure (i.e., whether the fracture is brittle or ductile), various characterization techniques were developed. Summaries of the various techniques that are available for polymer testing are summarized in Mai et al.[11] As discussed later, all the FR filled PP composites failed in a brittle manner when subjected to impact testing. Therefore, the impact fracture toughness measurement scheme based on LEFM analysis was employed.[12–14] The method involved the measurement of the impact fracture energy (U) as a function of the crack length (a) by using conventional impact testing techniques. From Figure 1 it can be seen that $a = D - l$. In the fracture mechanics analysis, all the cracks were sharpened by a fresh razor blade before the actual crack length was measured. The energy absorbed to fracture the specimen (U) is related to the sample geometry by[12]

$$U = G_C BD\phi + E_k \quad (2)$$

where B and D are the thickness and width of the specimen, respectively; ϕ is a geometry dependent calibration factor that depends on a[12]; and E_k is the kinetic energy loss. In eq. (2) the G_C is the impact fracture toughness of the material, which is also termed the critical strain energy release rate.

Both types of impact tests (i.e., conventional Charpy impact test and dynamic G_C) were carried out by using a Ceast Fractovis instrumented drop weight impactor tester. The same specimen geometry as shown in Figure 1 was used for both types of impact tests. The major differences are summarized in Table II.

Fractography

The tensile, impact, and cryogenic fractured surfaces were investigated by means of scanning electron microscopy (SEM, Jeol JSM-820). Cryogenic fractured surfaces were obtained by immersing the unbroken samples into liquid nitrogen for several minutes and breaking them with the tap of a hammer. All the fracture surfaces were gold coated before SEM examination.

RESULTS AND DISCUSSION

Limiting Oxygen Index (LOI) Measurements

The plots of LOI as a function of FR concentration for the PP composites filled with both types of FRs

Table II Major Differences between Conventional Charpy Impact Test and Dynamic G_C Measurement

	Charpy Test	Dynamic G_C
Crack length	Fixed	Varied
Crack tip	Finite radius	Sharpened by razor blade

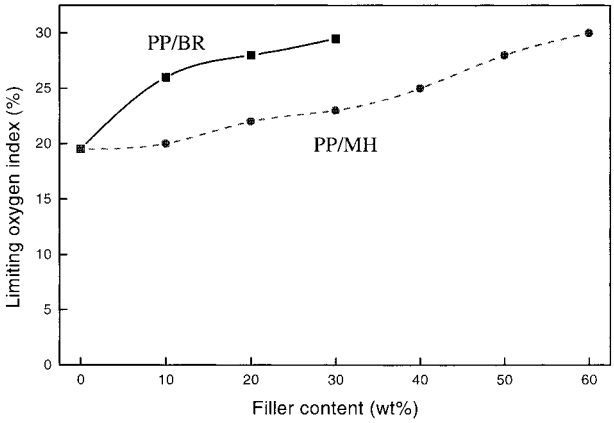

Figure 2 The effect of the flame retardant concentration on the LOI for PP/BR and PP/MH composites.

are illustrated in Figure 2. In both PP/BR and PP/MH systems the LOI increased as the FR content increased. This revealed that higher oxygen content was required to initiate and sustain combustion of the samples after the addition of FRs into the PP matrix. However, the improvement in the LOI was more rapid in the PP/BR system. The LOI at 30 wt % of BR and MH was 29.5 and 23%, respectively. It can thus be concluded that the BR system was more effective than MH as a FR. Higher loading of MH was necessary in order to provide adequate flame retardancy.

From Figure 2 it can be seen that in order for the PP/MH composite to have the same level of flame retardancy as the BR-30 composite (i.e., LOI = 29.5%), the MH concentration needed was 60 wt %. Therefore, the maximum concentrations of BR and MH employed in this investigation were 30 and 60 wt %, respectively.

Tensile Test

Typical tensile stress–strain curves for the PP/BR and PP/MH composites are shown in Figure 3. (The origin of each curve was shifted horizontally for clarity.) The same stress–strain curve for the PP homopolymer is included in both parts. The PP homopolymer and all the PP/BR composites investigated (up to the maximum BR content of 30 wt %) could be elongated up to 120% of the tensile strain without fracturing [Fig. 3(a)]. Their behaviors showed the typical characteristics for ductile polymers: stress whitening followed by necking and drawing.

Similar ductile behavior was also obtained in the MH-10 sample [Fig. 3(b)]. When the amounts of MH added up to 20 wt %, a ductile to quasi-brittle fracture transition occurred. Truly brittle behaviors resulted in the MH-50 and MH-60 samples in which the tensile specimens fractured in the linear elastic region of the stress–strain curves [Fig. 3(b)]. It can thus be concluded that when the maximum recommended level of BR was applied (i.e., 30 wt % of BR), the PP/BR composites still behaved in a ductile manner under tensile loading. For the PP/MH composites, they became highly brittle when the MH content was higher than 30 wt %.

Tensile modulus is an important parameter commonly used to characterize the stiffness of

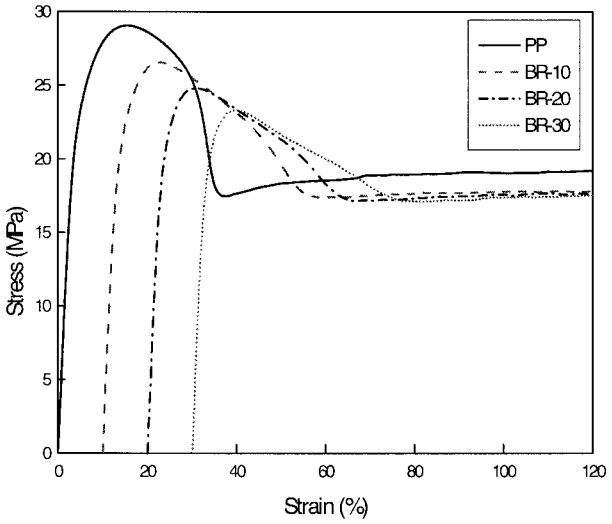

(a)

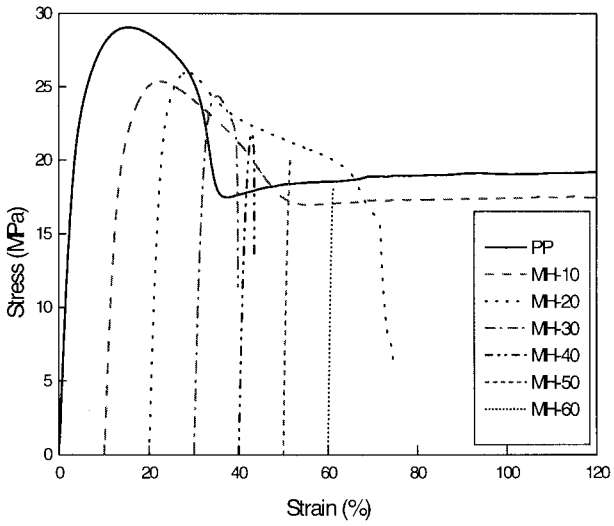

(b)

Figure 3 The tensile stress–strain curves for (a) PP/BR and (b) PP/MH composites.

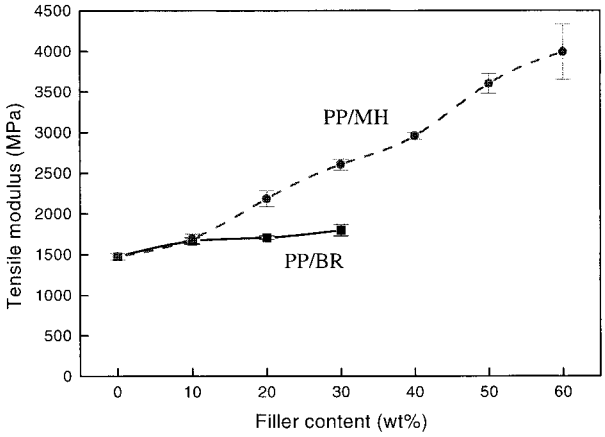

Figure 4 The effect of the flame retardant concentration on the tensile modulus for PP/BR and PP/MH composites.

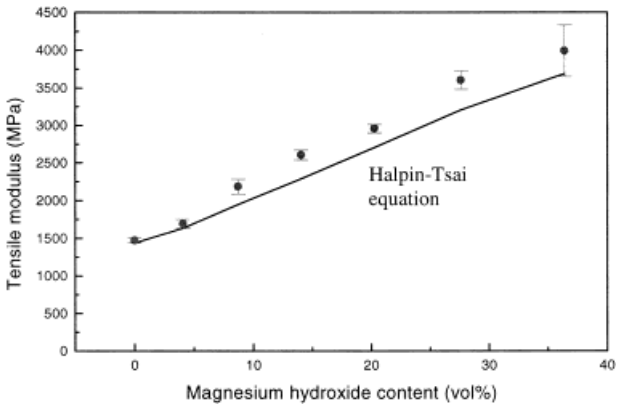

Figure 5 A comparison of the Halpin–Tsai equation and the experimentally measured tensile modulus for the PP/MH system.

materials. Figure 4 illustrates the effect of the FR concentration on the tensile modulus for both PP/BR and PP/MH systems. Similar trends were observed in both systems. The tensile modulus increased nonlinearly with increasing FR concentration. However, the change in modulus was more pronounced for the PP/MH system. The tensile modulus at 30 wt % of BR was 1.8 GPa, while it was 2.6 GPa in the PP/MH system with the same filler concentration. With a further increase of the MH concentration to 60 wt % the tensile modulus increased to 4.0 GPa, which corresponded to about 2.7 times that for the base PP homopolymer.

The tensile modulus (E_C) for the PP/MH composites was predicted by using the Halpin–Tsai equations[15]:

$$E_C = \frac{1 + \xi\eta V_f}{1 - \eta V_f} \times E_m$$

$$\eta = \frac{(E_f/E_m) - 1}{(E_f/E_m) + \xi} \qquad (3)$$

where E_f and E_m are the tensile modulus for the filler particle and matrix, respectively; V_f is the volume fraction of the filler particles; and $\xi = 2$ for spherical filler particles. A comparison of the Halpin–Tsai equation and the experimentally measured tensile modulus for the PP/MH system is given in Figure 5. A good correlation can be seen to exist between eq. (3) and the experimental values. For the PP/BR system the Halpin–Tsai prediction was not carried out because the BR was a mixture of two components: brominated phosphate ester and antimony trioxide.

Among the mechanical properties, yield strength is of primary importance. For ductile polymers it gives the information on the maximum allowable load before necking. Figure 6 shows the relationship between the tensile yield strength and the FR content for both PP/MH and PP/BR systems. It is clear from the tensile stress–strain curves [Fig. 3(a,b)] that, irrespective of the FR system, the specimens failed in a ductile manner (i.e., with prominent yield drop) when the FR content was low (i.e., ≤30 wt %). For the PP/MH system a further increase in the FR content (i.e., >30 wt %) resulted in the brittle failure of the specimens with the specimens fractured

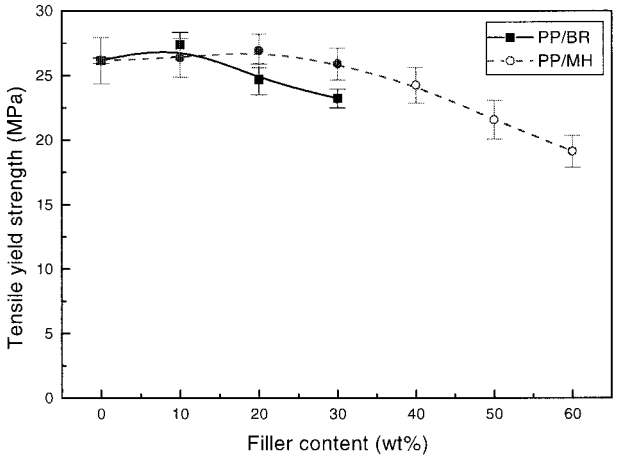

Figure 6 The variation of the tensile yield strength with the flame retardant content for both PP/MH and PP/BR systems. The solid symbols represent specimens failed in a ductile manner, and the open symbol represents specimens failed in a brittle manner.

catastrophically before yield drop [Fig. 3(b)]. Once brittle fracture occurred (i.e., MH content > 30 wt %) the tensile strength of the PP/MH system decreased with increasing MH content.

Even though both PP/MH and PP/BR systems failed in a ductile manner with low FR content (i.e., ≤30 wt %), their behaviors were totally different. The tensile yield strength for the PP/MH system was independent of the MH content. This implied a relatively strong interfacial bonding between the MH particle and the PP matrix. The tensile yield strength for the PP/BR system decreased with increasing BR content. This was due to the relatively weak interfacial bonding between the two component BR particles and the PP matrix.

Figure 7 presents SEM micrographs showing the longitudinally cryogenic fractured necking region of the BR-10 and MH-10 composites after tensile testing. It can be seen that both types of FR particles remained rigid, and the PP matrix was severely deformed and drawn around the rigid particles. A description of the deformation processes for the formation of the morphologies observed in Figure 7 is illustrated in Figure 8. Initial debonding due to the applied tensile stress occurred at the pole of the filler particles. With increased loading the filler–matrix interfacial debonding surface area increases; hence, voids form at the interfacial debonding region. Subsequently, the voids coalesce and the PP ligaments between filler particles are cold drawn and form into the morphology shown in Figure 7.

A SEM micrograph showing the longitudinally cryogenic fractured necking region of a BR-30 sample is presented in Figure 9. The morphology was formed by the mechanisms illustrated in Figure 8. It is worthwhile to point out that the filler particles in the BR-30 specimen (Fig. 9) were significantly bigger than in the BR-10 specimen [Fig. 7(a)]. This indicated that the BR fillers agglomerated for the specimens with higher filler content.

Figure 10 shows the longitudinally cryogenic fractured surface at a region close to the tensile fractured region of a MH-40 sample. As mentioned previously, the tensile stress–strain behavior was brittle in nature with such a MH content. It can be seen from Figure 10 that filler/PP debonding was totally absent, which was in sharp contrast to the ductile fracture behavior of the MH-10 sample [Fig. 7(b)]. It can also been observed from Figure 10 that the MH particles were very well bonded to the PP matrix. This supported the assumption that the interfacial bond strength between the MH particles and PP matrix is relatively strong.

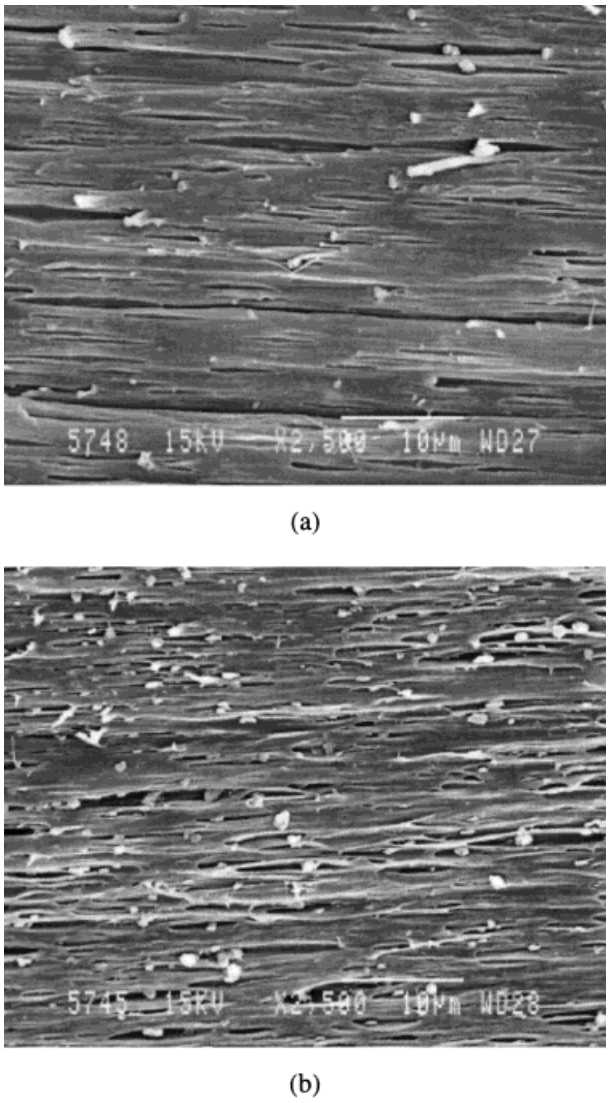

Figure 7 SEM micrographs showing the longitudinally cryogenic fractured necking region of the flame retardant filled PP composites: (a) BR-10 and (b) MH-10.

Figure 11 shows the tensile fracture surfaces for the PP/MH composites with MH content varied from 20 to 60 wt %. For the composites with low MH content, such as the MH-20 and MH-30 composites (Fig. 11), a high density of PP fibrils was seen. These PP fibrils were remnants of the cold-drawn PP ligaments between the rigid MH particles (see Fig. 8). By going through the sequence of SEM micrographs in Figure 11, it is clear that the density of PP fibrils decreased with

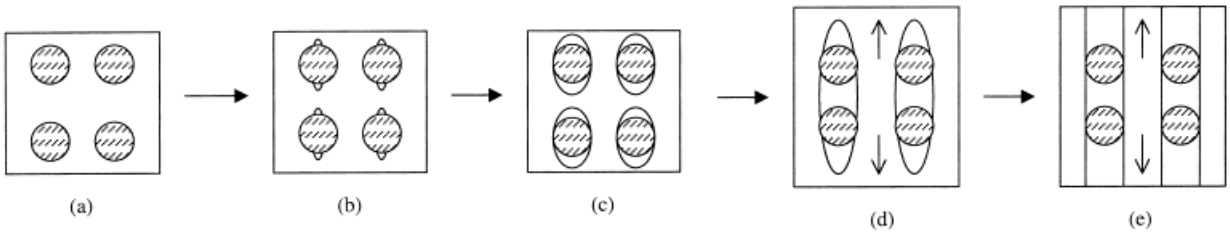

Figure 8 A schematic illustration of the mechanisms in the tensile yielding of the flame retardant filled PP composites with low filler content: (a) rigid particulate fillers in the PP matrix, (b) initial debonding under tensile loading, (c) void growth due to growth in debonding, (d) coalescence of voids, and (e) drawing of PP ligaments.

increasing MH content. At 60 wt % of MH the formation of cold-drawn PP fibrils was totally prohibited [Fig. 11(e)].

Charpy Impact Test

The Charpy impact strengths [see eq. (1)] for both PP/BR and PP/MH composites are shown in Figure 12. Observe that the impact strength for the two systems behaved differently as the filler contents were increased up to 30 wt %. For the PP/BR composites the impact strength increased slightly with increasing filler content (up to 30 wt %). For the PP/MH composites, although a slight improvement in the impact strength was also observed for the filler content up to 30 wt %, the improvement was not as high as in the PP/BR composites. With a further increase in the filler content in the PP/MH composite (i.e., 40 wt % and above) the impact strength was suddenly significantly reduced. The effect of fillers on the notched impact strength of PP is known to depend on a number of factors.[16,17] Among these, the filler particle geometry, filler size and its distribution, filler–matrix interfacial adhesion, and spatial distribution are known to be influential.[18,19]

The impact fracture surface for a BR-30 sample is shown in Figure 13. The interfacial bonding between the BR filler and PP matrix was very weak as reflected by the severe interfacial debonding observed. A consequence of the weak filler–matrix interface was the possibility of matrix cracking. A matrix crack initiated from the filler–matrix debonding can be seen in the top right corner of Figure 13. The filler–matrix interface was stronger for the PP/MH composite (Fig. 14). Vollenberg and Heikens[17] observed that in chalk filled PP composites the strong interfacial bonding can lead to a decrease in the impact strength with increasing filler content. In poor in-

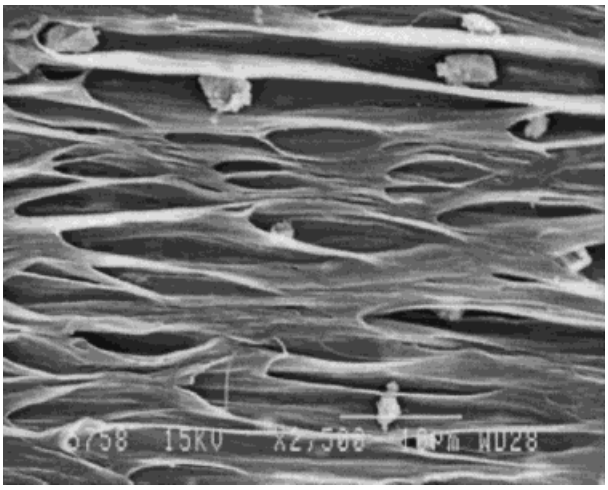

Figure 9 SEM micrographs showing the longitudinally cryogenic fractured necking region of a BR-30 specimen.

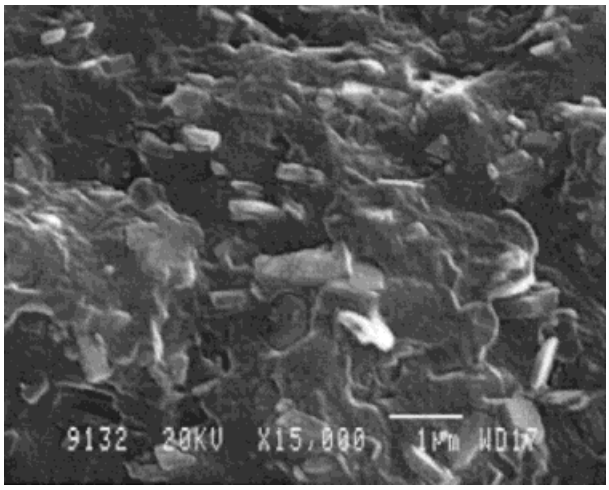

Figure 10 SEM micrographs showing the longitudinally cryogenic fractured necking region of a MH-40 specimen.

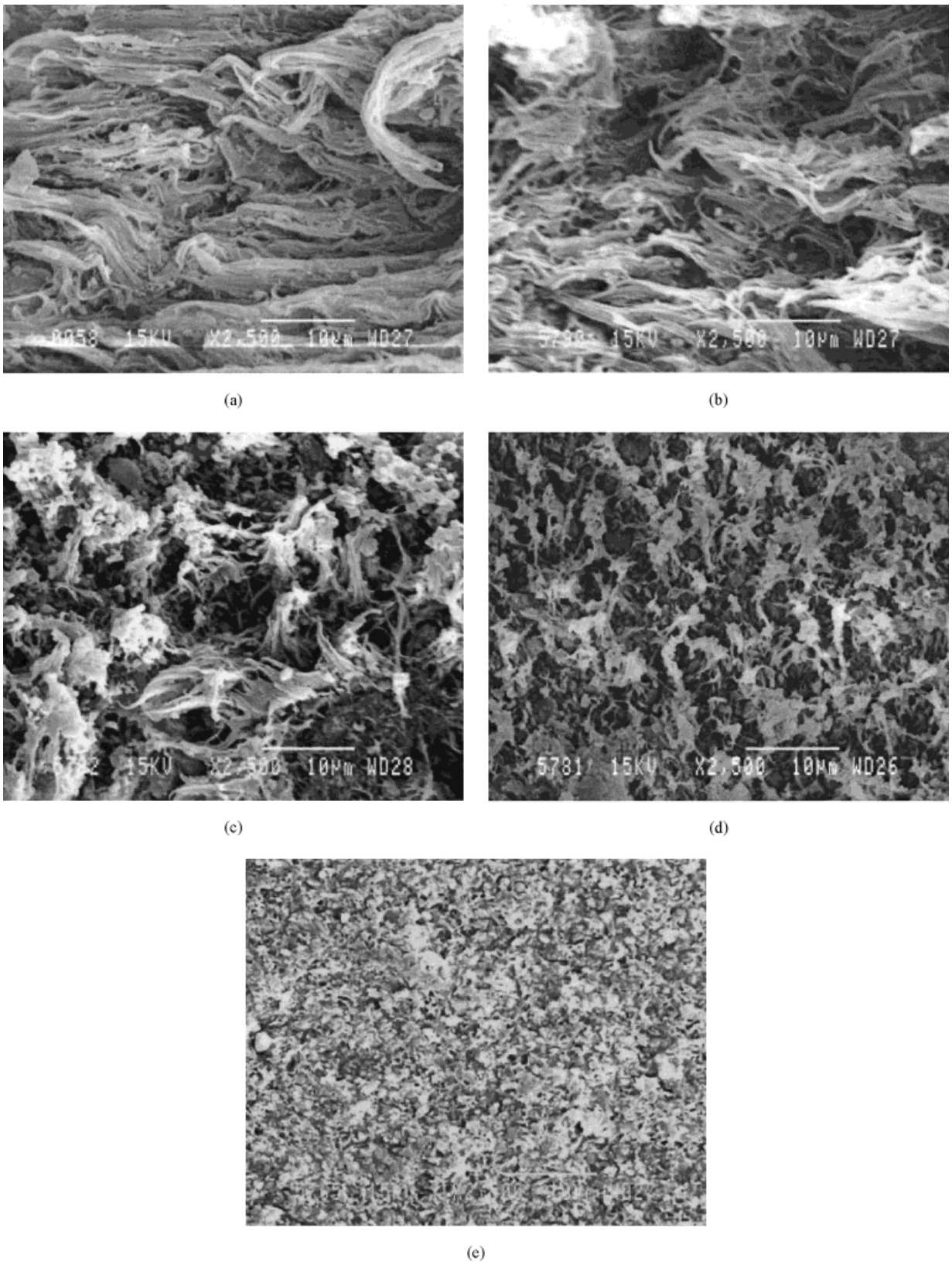

Figure 11 Tensile fracture surfaces of the PP/MH composites: (a) MH-20, (b) MH-30, (c) MH-40, (d) MH-50, and (e) MH-60.

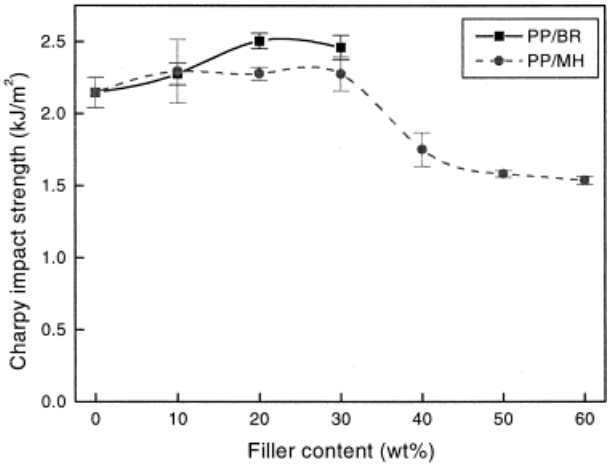

Figure 12 The Charpy impact strength for PP/BR and PP/MH composites.

terfacial bonding a maximum in impact strength was observed with increasing filler content, and the location of the maximum depended on the particle size of the filler.[17]

In our impact test results (Fig. 12) and microscopic observations (Figs. 13, 14) we concluded that a weak filler–matrix interface (i.e., the PP/BR composites) promoted filler–matrix debonding and matrix cracking. These enhanced the impact strength of the composites. For the systems with a good filler–matrix interface the reduced number of fracture energy absorption mechanisms lowered the impact strength.

Impact Fracture Toughness Measurement

The plots of the impact fracture energy against $BD\phi$ for various material systems are shown in Figure 15. A straight-line relationship was obtained by the method of least squares. The slope and the corresponding vertical intercept of each curve gave the G_C and the E_k as required. The measured G_C values as a function of FR are summarized in Figure 16. From the figure it can be seen that the G_C decreased rapidly for both PP/BR and PP/MH composites with the addition of 10 wt % of filler. Further increasing the filler content to 20 wt % caused the G_C to increase slightly. When the amount of FR was further increased, say 30 wt % and higher, different results were obtained from the two systems. The G_C continued to increase for the BR-30 sample. However, the G_C decreased with increasing MH content in the PP/MH composites.

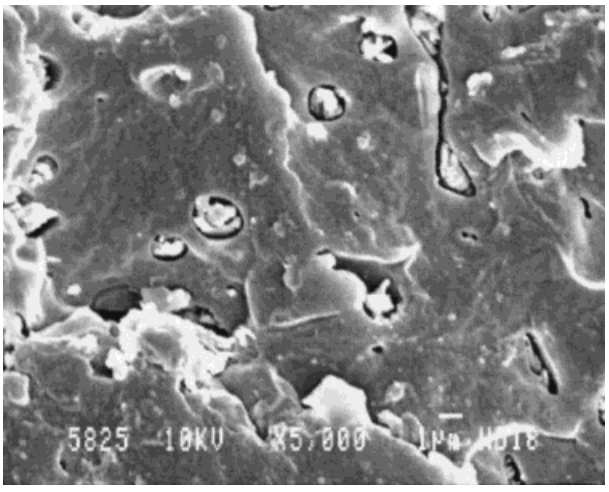

Figure 13 The impact fracture surface for a BR-30 sample showing the poor interfacial adhesion between the filler particle and PP matrix.

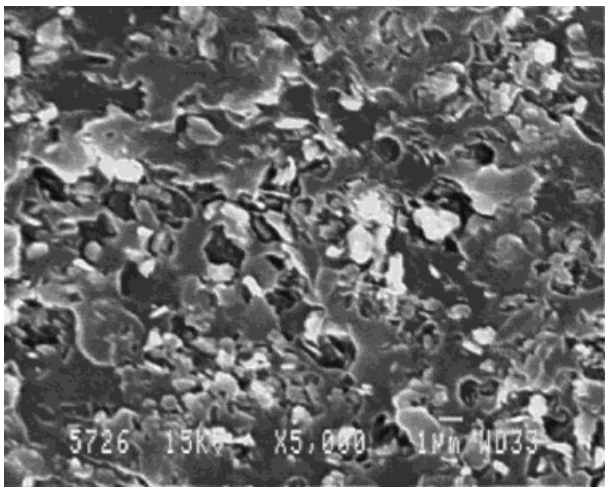

Figure 14 The impact fracture surface of a MH-10 sample showing good interfacial adhesion between the filler particle and PP matrix.

A comparison of Figures 12 and 16 shows that the S_I was higher than the corresponding G_C values. There were two reasons for the discrepancy. The first reason was related to the different notch tip geometry. As mentioned earlier, the overall specimen geometry used in both impact tests was the same except a blunt notch was used in the Charpy impact test and a razor sharpened crack was used in the impact G_C measurement. The main purpose of having a sharp crack instead of a blunt notch was to measure the true crack propagation energy in the G_C measurement. In the Charpy impact test, energy was needed to initiate a sharp crack from the blunt notch, as well as to propagate the crack.

The second reason for the difference between the S_I and G_C was due to kinetic energy loss.

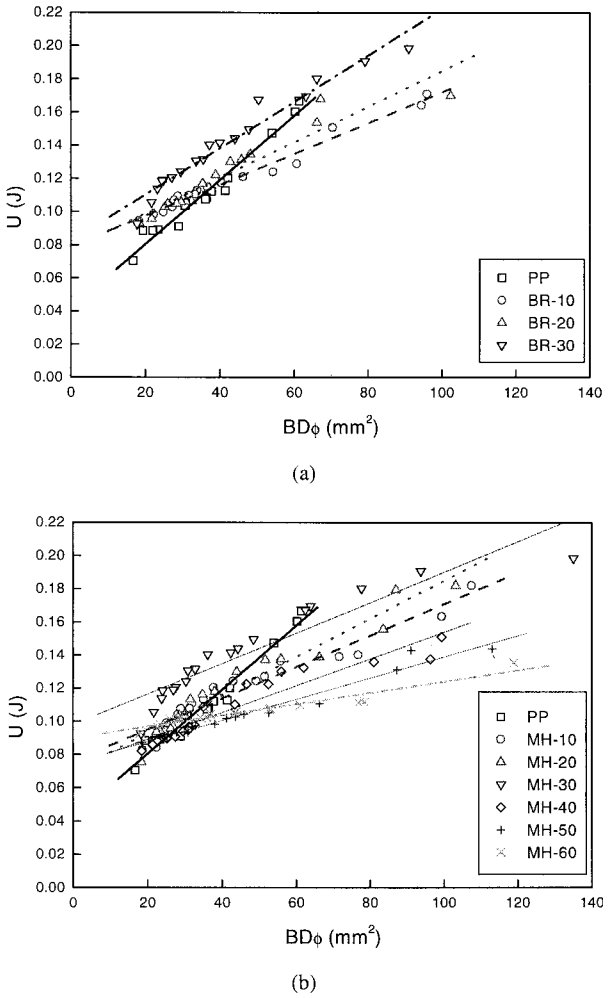

Figure 15 The impact energy (U) versus the $BD\phi$ plots for the flame retardant filled PP composites: (a) PP/BR and (b) PP/MH.

From eq. (2) it can be seen that in the G_C measurement the measured total energy consisted of two terms: the fracture surface related term (i.e., $G_C BD\phi$) and the kinetic energy term (i.e., E_k). The E_k can be obtained from the vertical intercept of the U against $BD\phi$ plot (Fig. 15). The E_k can be interpreted as the kinetic energy carried by the two broken halves of the specimens as they were propelled away from the supporting anvil. In the Charpy impact test the measured total impact energy was the sum of the crack initiation energy (E_I), crack propagation energy (E_P), and E_k.

From Figure 15 the E_k was obtained from the vertical intercept of the U against $BD\phi$ plots for the respective FR filled PP composites and PP homopolymer. The E_k was then subtracted from the respective Charpy impact strengths given in

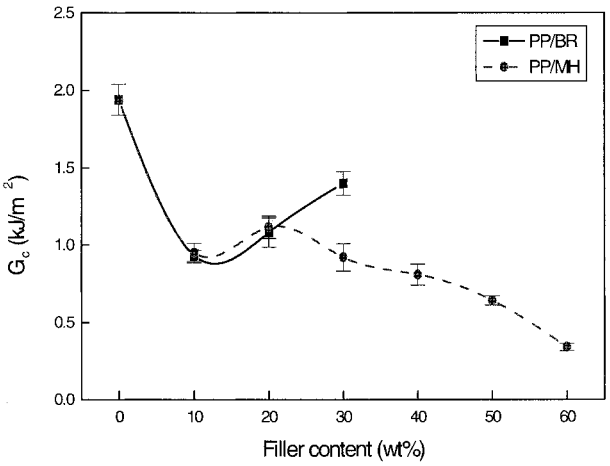

Figure 16 The impact fracture toughness (G_C) versus the filler content for PP/BR and PP/MH composites.

Figure 12 to give the kinetic energy corrected Charpy impact strength ($S_{I\text{corr}}$):

$$S_{I\text{corr}} = S_I - E_k \tag{4}$$

The $S_{I\text{corr}}$ values for the composites are shown in Figure 17. It can be seen that after the kinetic energy correction the $S_{I\text{corr}}$ was in better agreement with the G_C plot in Figure 16.

CONCLUSION

The LOIs for a PP homopolymer modified by two types of FR fillers were investigated and compared. The BR system was more effective than the

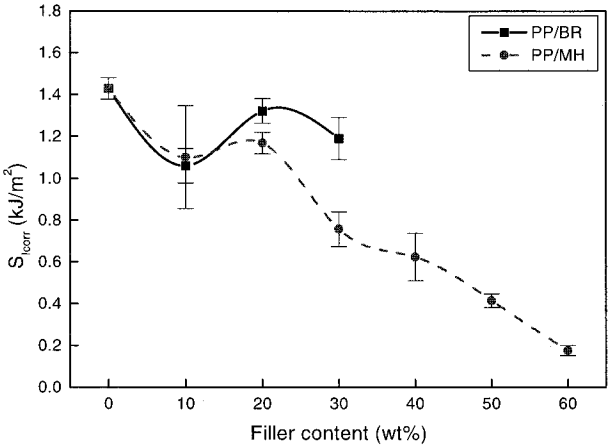

Figure 17 The kinetic energy corrected Charpy impact strength ($S_{I\text{corr}}$) versus the filler content for both PP/BR and PP/MH composites.

MH system because 60 wt % of MH was needed to attain the same LOI value as a PP/BR composite containing 30 wt % of FR filler. The mechanical properties of the two types of FR filled PP were also investigated. The additions of both types of FRs can improve the stiffness of PP. The tensile yield strength for the PP/MH composites was higher than that for the PP/BR composites due to the stronger interfacial bond strength for the PP/MH composites. However, the weaker filler–matrix interfacial bond in the PP/BR composites gave rise to the higher fracture toughness due to energy absorption by filler–matrix debonding and matrix cracking.

The first author is the recipient of a Research Studentship and a Research Tuition Scholarship from the City University of Hong Kong.

REFERENCES

1. Rothon, R. N. Particulate-Filled Polymer Composites: Longmans, Harlow: New York, 1995.
2. Hastie, J. W. J Natl Burn Stand 1973, 77A, 733.
3. Edenbaum, J. Plastics Additives and Modifiers Handbook; Van Nostrand Reinhold: New York, 1992.
4. Wooley, W. D.; Fardell, P. J. Fire Safety J 1982, 5, 29.
5. Reinke, R. E.; Reinhardt, C. F. Mod Plast 1983, 50, 94.
6. Katz, H. S.; Milewski, J. V. Handbook of Fillers and Reinforcements for Plastics; Van Nostrand Reinhold: New York, 1978.
7. Hornsby, P. R.; Watson, C. L. Plast Rubber Process Applic 1989, 11, 45.
8. Rothon, R. N.; Hornsby, P. R. Polym Degrad Stabil 1996, 54, 383.
9. Hornsby, P. R. Fire Mater 1994, 18, 269.
10. Crawford, R. J. Polymer Engineering, 2nd ed.; Pergamon: New York, 1990.
11. Mai, Y. W.; Wong, S. C.; Chen, X. H. In Polymer Blends Volume 2: Performance; Paul, D. R., Bucknall, C. B., Eds.; Wiley-Interscience: New York, 2000.
12. Plati, E.; Williams, J. G. Polym Eng Sci 1975, 15, 69.
13. Tam, W. Y.; Cheung, T.; Li, R. K. Y. Polym Test 1996, 15, 363.
14. Li, W. D.; Li, R. K. Y.; Tjong, S. C. Polym Test 1997, 16, 563.
15. Hull, D.; Clyne, T. W. An Introduction to Composite Materials, 2nd ed.; Cambridge University Press: New York, 2000.
16. Liang, J. Z.; Li, R. K. Y. Polym Compos 1998, 19, 698.
17. Vollenberg, P. H. T.; Heikens, D. J Mater Sci 1990, 25, 3089.
18. Liu, Z. H.; Li, R. K. Y.; Tjong, S. C.; Qi, Z. N.; Wang, F. S.; Choy, C. L. Polymer 1998, 39, 4433.
19. Liu, Z. H.; Li, R. K. Y.; Tjong, S. C.; Choy, C. L.; Zhu, X. G.; Qi, Z. N.; Wang, F. S. Polymer 1999, 40, 2903.